

Cite this: *Chem. Soc. Rev.*, 2011, **40**, 2494–2507

www.rsc.org/csr

CRITICAL REVIEW

Metamaterials: a new frontier of science and technology

Yongmin Liu^a and Xiang Zhang^{*ab}

Received 30th April 2010, Accepted 19th November 2010

DOI: 10.1039/c0cs00184h

Metamaterials, artificial composite structures with exotic material properties, have emerged as a new frontier of science involving physics, material science, engineering and chemistry. This *critical review* focuses on the fundamentals, recent progresses and future directions in the research of electromagnetic metamaterials. An introduction to metamaterials followed by a detailed elaboration on how to design unprecedented electromagnetic properties of metamaterials is presented. A number of intriguing phenomena and applications associated with metamaterials are discussed, including negative refraction, sub-diffraction-limited imaging, strong optical activities in chiral metamaterials, interaction of meta-atoms and transformation optics. Finally, we offer an outlook on future directions of metamaterials research including but not limited to three-dimensional optical metamaterials, nonlinear metamaterials and “quantum” perspectives of metamaterials (142 references).

1. Introduction

The property of a bulk material is essentially determined by the chemical elements and bonds in the material. People have never ceased from better understanding and controlling material properties. For instance, over 3000 years ago, our ancestors already knew how to synthesize alloys to improve the mechanical properties of metals. The conductivity of silicon can be orders of magnitude higher by slight doping, laying the foundation for the whole semiconductor industry formed around 1960. Most recent nanoscience and nanotechnology aim to study the electronic, optical, thermal and mechanical property of materials starting from the atom- or molecule-level. All of these efforts have significantly expanded the range of materials accessible to people.

In the past decade, metamaterials offered an entirely new route to further enhance the capability of people to design material properties at will.^{1,2} Different from the aforementioned examples, the physical properties of metamaterials are not primarily dependent on the intrinsic properties of the chemical constituents, but rather on the internal, specific structures of metamaterials. These artificial structures function as atoms and molecules in traditional materials; while through regulated interactions with electromagnetic (EM) waves, they can produce fascinating physical properties unavailable in naturally occurring or chemically synthesized materials. This is why such composite structures are termed metamaterials, which literally stand for materials beyond natural ones.

In the review articles,^{1,2} the basic concept and theory of metamaterials and research advances up to year 2005 in this area are nicely presented. As proof-of-principle demonstrations, at the early stage most research focused on metamaterials in the microwave region to implement artificial magnetism, negative refractive index, negative refraction and superlens (see ref. 1 and 2, and references therein). Within the past few years, metamaterials have rapidly advanced to terahertz and optical frequencies. Moreover, new subareas of metamaterials research have emerged, and prototype devices based on metamaterials have been demonstrated. This review aims to cover both the fundamentals of metamaterials as well as the progress of metamaterials research since 2005, serving as a springboard to further reading. We will concentrate on electromagnetic metamaterials in this review, although the concept of metamaterials has been successfully applied to acoustics.^{3,4}

In electromagnetism, electric permittivity (ϵ), and magnetic permeability (μ) are the two fundamental parameters characterizing the EM property of a medium.⁵ Physically, permittivity (permeability) describes how an electric (magnetic) field affects, and is affected by a medium, which is determined by the ability of a material to polarize in response to the electric (magnetic) field. We use the “material parameter space” as shown in Fig. 1 to represent all materials, as far as EM properties are concerned. Region I in the upper-right quadrant covers materials with simultaneously positive permittivity and permeability, which include most dielectric materials. Quadrant II embraces metals, ferroelectric materials, and doped semiconductors that could exhibit negative permittivity at certain frequencies (below the plasma frequency). Region IV is comprised of some ferrite materials with negative permeability, the magnetic responses of which,

^a *NSF Nanoscale Science and Engineering Center (NSEC), University of California, 3112 Etcheverry Hall, Berkeley, CA 94720, USA. E-mail: xiang@berkeley.edu*

^b *Materials Science Division, Lawrence Berkeley National Laboratory, 1 Cyclotron Road, Berkeley, CA 94720, USA*

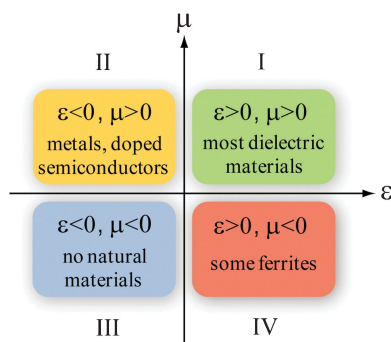


Fig. 1 Material parameter space characterized by electric permittivity (ϵ) and magnetic permeability (μ).

however, quickly fade away above microwave frequencies. The most interesting region in the material parameter space is quadrant III, in which permittivity and permeability are simultaneously negative. In nature there is no such material.

Yet, the material with simultaneously negative permittivity and permeability possesses many remarkable properties, which were theoretically investigated in detail by Veselago more than forty years ago.⁶ Let us consider a monochromatic plane wave propagating in an isotropic, homogenous medium. The electric and magnetic components of the plane wave have the form as $\vec{E}(\omega, \vec{k}) = \vec{E}_0 \exp(i\vec{k} \cdot \vec{r} - i\omega t)$ and $\vec{H}(\omega, \vec{k}) = \vec{H}_0 \exp(i\vec{k} \cdot \vec{r} - i\omega t)$, respectively, where ω is the angular frequency and \vec{k} is the wave vector. If there are no free charges (ρ) and currents (\vec{j}), Maxwell's equations⁵

$$\nabla \cdot \vec{B} = 0, \nabla \times \vec{E} = -\frac{\partial \vec{B}}{\partial t} \quad (1)$$

$$\nabla \cdot \vec{D} = \rho, \nabla \times \vec{H} = \vec{j} + \frac{\partial \vec{D}}{\partial t}$$

and constitutive equations

$$\begin{cases} \vec{D} = \epsilon \vec{E} = \epsilon_0 \epsilon_r \vec{E} \\ \vec{B} = \mu \vec{H} = \mu_0 \mu_r \vec{H} \end{cases} \quad (2)$$

can be simplified into

$$\begin{cases} \vec{k} \times \vec{E} = \mu \omega \vec{H} \\ \vec{k} \times \vec{H} = -\epsilon \omega \vec{E} \end{cases} \quad (3)$$

Here \vec{D} (\vec{B}) is the electric (magnetic) induction, ϵ_0 (μ_0) is the permittivity (permeability) of vacuum, and ϵ_r (μ_r) is the relative permittivity (permeability) of a medium. From eqn (3), it can be readily seen that \vec{k} , \vec{E} and \vec{H} form a right-handed triplet of vectors, as a plane wave propagates in normal dielectric materials with $\epsilon > 0$ and $\mu > 0$. In contrast, these vectors form a left-handed triplet in materials with $\epsilon < 0$ and $\mu < 0$. Moreover, the Poynting vector, defined as $\vec{S} = \vec{E} \times \vec{H}$, is antiparallel to the wave vector \vec{k} in such materials (Fig. 2). It is further proved that the phase refractive index given by $n = \pm \sqrt{|\epsilon_r| |\mu_r|}$ must take a negative sign, so that the causality is still conserved.⁶ Due to the aforementioned exotic properties, materials with simultaneously negative permittivity and permeability are called left-handed materials (LHMs), or

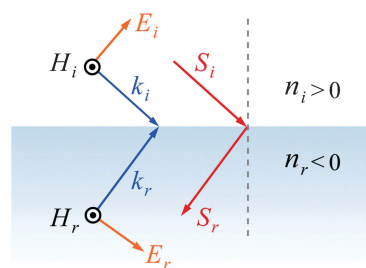


Fig. 2 Schematic of negative refraction at the interface between a positive-index material and a negative-index material. Note in the negative-index material, the wave vector (\vec{k}) and Poynting vector (\vec{S}) are antiparallel; while in the positive-index material, they are parallel.

negative-index materials (NIMs). Positive-index materials are abbreviated as PIMs in this paper.

Negative-index materials give rise to a host of counter-intuitive phenomena as Veselago discussed in his seminal paper.⁶ For example, if light is incident from a positive-index material to a negative-index one, the refracted light lies on the same side as the incident light with respect to the surface normal, because of the causality principle and conservation of tangential wave vectors (Fig. 2). In other words, the refracted light bends negatively at the interface. From Snell's law⁵

$$\frac{\sin \theta_i}{\sin \theta_r} = \frac{n_r}{n_i}, \quad (4)$$

the angle of refraction is indeed negative when the refractive indices of the two materials are opposite in signs, as illustrated in Fig. 2. This is in striking contrast to normal cases in which only positive-index materials are involved. Moreover, the Doppler effect and Cherenkov effect are also reversed in NIMs.⁶

However, there are no natural materials exhibiting negative refractive indices. Therefore Veselago's theoretical work on NIMs hibernated for a long time. It is Pendry *et al.*, who first proposed to use artificial materials^{7,8} to fully expand the available range of material properties (including the negative refractive index) as shown in Fig. 1, and opened up a completely new research area—metamaterials.

2. Engineering electric and magnetic responses by metamaterials

In classical electromagnetics, usually the material property can be well described by the Drude–Lorentz model, which can be derived from the oscillation equation of electric charges or fictitious magnetic charges driven by an external EM wave.⁵ Due to the symmetry of EM waves, the frequency-dependent permittivity and permeability follow very similar formula,

$$\begin{cases} \epsilon_r(\omega) = 1 - \frac{\omega_{p,e}^2}{\omega^2 - \omega_{0,e}^2 + i\gamma_e \omega} \\ \mu_r(\omega) = 1 - \frac{\omega_{p,m}^2}{\omega^2 - \omega_{0,m}^2 + i\gamma_m \omega} \end{cases} \quad (5)$$

Here ω_p is the plasma frequency, ω_0 is the resonant frequency, and γ is the damping factor related to material losses. The subscripts e and m represent electric and magnetic response,

respectively. Substituting proper values into eqn (5), we can characterize material properties over a wide frequency range from microwave to optical. For noble metals, $\omega_{p,e}$ is at visible or UV frequency and $\omega_{0,e}$ is taken as zero under the free electron approximation. This means that the permittivity of metals is always negative below the plasma frequency. On the other hand, naturally existing materials that exhibit magnetic responses with negative permeability are far less common than those that exhibit electric responses. This is particularly true when we move beyond the gigahertz region, where the magnetic response of most materials begins to tail off. The fundamental reason for rare magnetic materials at high frequencies is that magnetic polarization originates from either the flow of orbital currents or unpaired electron spins, but both effects only respond to EM waves at low frequencies.⁹ In the optical regime, $\mu = 1$ holds for all naturally existing materials.

Metamaterials allow us to surmount obstacles of nature, leading to complete freedom to engineer material properties.^{1,2} Metamaterials consist of periodically or randomly distributed structured elements, whose size and spacing are much smaller than the wavelength (λ) of EM waves. As a result, the microscopic detail of each individual structure cannot be sensed by EM waves. What matters is the average result of the collective response of the whole assembly. In other words, such a collection of inhomogeneous objects can be characterized by an equivalent homogenous material with effective relative permittivity ($\epsilon_{r,\text{eff}}$) and permeability ($\mu_{r,\text{eff}}$) at the macroscopic level. The most attractive aspect of metamaterials is that $\epsilon_{r,\text{eff}}$ and permeability $\mu_{r,\text{eff}}$ can be controlled, using properly designed structures.

In 1996, Pendry *et al.* proposed dilute metals with extremely low plasma frequency.⁷ The structure is a three-dimensional (3D) lattice of very thin metallic wires, as schematically shown in Fig. 3(a). Such a structure gives rise to two effects. First, the effective electron density is apparently reduced. Second, the effective electron mass is increased because of the self-inductance of the wire structure. Detailed calculations show that the effective relative permittivity of the system still obeys the Drude–Lorentz model as

$$\epsilon_{r,\text{eff}}(\omega) = 1 - \frac{\omega_{p,\text{eff}}^2}{\omega(\omega + i\gamma_{\text{eff}})}. \quad (6)$$

In eqn (6), the effective plasma frequency and damping factor are given by

$$\omega_{p,\text{eff}}^2 = \frac{n_{e,\text{eff}}e^2}{\epsilon_0 m_{e,\text{eff}}} = \frac{2\pi c^2}{d^2 \ln(d/r)} \quad (7)$$

and

$$\gamma_{\text{eff}} = \frac{\epsilon_0 d^2 \omega_p^2}{\pi r^2 \sigma} \approx 0.1 \omega_{p,\text{eff}}, \quad (8)$$

respectively, where σ is the conductivity of metal (typically in the order of $10^7 \Omega^{-1} \text{ m}^{-1}$). Considering the wire radius $r = 1.0 \times 10^{-6} \text{ m}$, lattice constant $d = 3.5 \times 10^{-3} \text{ m}$, one can obtain the effective plasma frequency $\omega_{p,\text{eff}} = 7.52 \times 10^{10} \text{ rad s}^{-1}$, five orders of magnitudes smaller than that of noble metals.

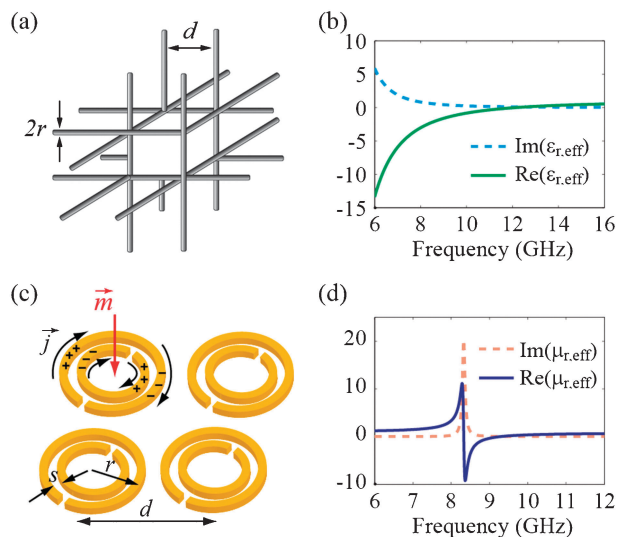


Fig. 3 Basic metamaterial structures to implement artificial electric and magnetic responses. (a) Schematic of periodic wires (with radius r) arranged in a simple cubic lattice (with lattice constant d). (b) Effective permittivity of wire media, acting as dilute metals with an extremely-low plasma frequency. (c) Schematic of split ring resonators, with outer radius r and separation s between the two rings. A magnetic field penetrating the resonator induces a current (\vec{j}), and thus a magnetic moment (\vec{m}). (d) Effective permeability of split ring resonators around the resonance frequency.

The effective permittivity of the metallic wire arrays is plotted in Fig. 3(b).

In terms of magnetism, it can be created if we produce a current loop like the orbital current in natural magnetic materials. Such a current can be generated, for example, by a time-varying magnetic field threading through a conducting coil, simply from Faraday's law. Although the induced current, and thus magnetic moment are normally weak, they can be dramatically enhanced when introducing resonances into the coil. Split ring resonators (SRRs) are one of the original designs for strong artificial magnetism.⁸ Each SRR is composed of two concentric split rings with the openings at the opposite directions as illustrated in Fig. 3(c). From the point of view of equivalent circuits, an SRR can be considered as an LC circuit with the natural resonant frequency given by $\omega_0 = \sqrt{1/LC}$, with L and C denoting the geometric inductance and capacitance of the SRR structure, respectively. Within a certain frequency region centred at ω_0 , the magnetic flux threading through an SRR induces a strong circulating current, resulting in an effective magnetic moment. This induced magnetic moment responds in phase or out of phase with respect to the external magnetic field. If the strength of the magnetic response is sufficiently strong, effective relative magnetic permeability $\mu_{r,\text{eff}}$ with a negative value can be achieved.

Detailed derivations show that the effective relative magnetic permeability of an SRR array is given by⁸

$$\mu_{r,\text{eff}}(\omega) = 1 - \frac{F\omega^2}{\omega^2 - \omega_0^2 + i\Gamma\omega} \quad (9)$$

where F is the filling ratio of the SRR

$$F = \frac{\pi r^2}{d^2} \quad (10)$$

ω_0 represents the resonance frequency

$$\omega_0 = \sqrt{\frac{3sc^2}{\pi^2 r^3}} \quad (11)$$

and Γ is the damping term

$$\Gamma = \frac{2}{r\sigma\mu_0} \quad (12)$$

As an example, we take the following parameters of SRRs: $d = 4 \times 10^{-3}$ m, $r = 1 \times 10^{-3}$ m, and $s = 1 \times 10^{-4}$ m. The resulting resonance is $f_0 = \omega_0/2\pi = 8.324$ GHz. It should be noted that this frequency corresponds to a free-space wavelength of 3.6 cm, about one order of magnitude larger than the lattice constant d . Such a deep subwavelength characteristic guarantees that the effective medium approximation is valid. Fig. 3(d) plots the effective permeability of an SRR around the resonant frequency f_0 , which exhibits a typical Drude–Lorentz feature. Indeed, $\mu_{r,\text{eff}}$ can be negative in such nonmagnetic conducting elements, if the damping is not large.

Very often, it is difficult to analytically derive the effective parameters of certain metamaterials, due to the complexity of the structure. Alternatively we can retrieve the effective parameters from numerical simulations.^{10–13} The first step of the retrieval procedure is to calculate the transmission and reflection of the composite metamaterials, based on numerical algorithms, such as Finite-Difference Time-Domain (FDTD) and Finite Element Method (FEM). Some commercial softwares, including CST Microwave Studio, COMSOL Multiphysics and ANSOFT HFSS, are widely used in the metamaterials research community. The refractive index and impedance are related to the transmission coefficient (t) and reflection coefficient (r) by equations:¹⁰

$$z_{\text{eff}} = \pm \sqrt{\frac{(1+r)^2 - t^2}{(1-r)^2 - t^2}} \quad (13)$$

$$n_{\text{eff}} = \pm \cos^{-1} \left[\frac{1}{k_0 L} \left(\frac{1-r^2+t^2}{2t} \right) \right] + \frac{2m\pi}{k_0 L} \quad (14)$$

where k_0 is the wave vector in vacuum defined as $k_0 = 2\pi/\lambda_0$, L is the thickness of the metamaterial, and m is an integer. We can correctly retrieve z_{eff} and n_{eff} from eqn (13) and (14),

considering that metamaterials are passive media, that is, the real part of z_{eff} and the imaginary part of n_{eff} have to be positive.¹⁰ Subsequently, $\epsilon_{r,\text{eff}}$ and $\mu_{r,\text{eff}}$ can be readily obtained according to $\epsilon_{r,\text{eff}} = n_{\text{eff}}/z_{\text{eff}}$ and $\mu_{r,\text{eff}} = n_{\text{eff}} \cdot z_{\text{eff}}$. It should be pointed out that the retrieval process is not trivial in general, especially when metamaterials are anisotropic or bi-anisotropic,¹¹ and light is obliquely incident.¹³

3. Negative index metamaterials and applications of metamaterials

By overlapping two sets of meta-structures with $\epsilon_{r,\text{eff}} < 0$ and $\mu_{r,\text{eff}} < 0$ in the same frequency window, we expect to create metamaterials with a negative effective refractive index (*i.e.*, $n_{\text{eff}} < 0$), which were first experimentally demonstrated by Smith and colleagues in the microwave domain.^{14,15} A wedge-shaped metamaterial sample consisting of periodic array of copper SRRs and wires was used to measure the refraction of a beam at the exit interface (Fig. 4(a)). Negative refraction was indeed observed in a manner consistent with Snell's law. Although there were fierce debates on the validity of the experimental results as well as the fundamental properties of NIMs, a series of experimental and theoretical work ambiguously prove the reality of NIMs.¹ Ever since then, considerable interest has been sparked in the field of metamaterials. Within several years, magnetic metamaterials, and consequently NIMs have been advanced from microwave frequencies to the visible region, by scaling down the structure size and taking prudent designs.^{16–18} Negative permeability is the heart of NIMs. To achieve magnetic resonance at optical frequencies, however, it is shown that the size of SRRs has to be smaller than 100 nanometres, and the gap is less than 10 nanometres. Furthermore, the amplitude of the resonant permeability from SRRs decreases and ultimately ceases to reach a negative value in the visible region.¹⁹ These challenges impelled researchers to seek alternative designs other than the combination of metallic wires and SRRs. The most successful optical NIMs so far are the fishnet structure,^{20–22} which consists of two layers of metal meshes separated by a dielectric spacer layer (Fig. 4(b)). The paired stripes that are oriented parallel to the electric field provide negative $\epsilon_{r,\text{eff}}$, while the other pairs of stripes parallel to the magnetic field offer negative $\mu_{r,\text{eff}}$. Since the thickness of the spacing dielectric is easy to control, the simple design of the fishnet structure significantly eases the fabrication burden, compared to the

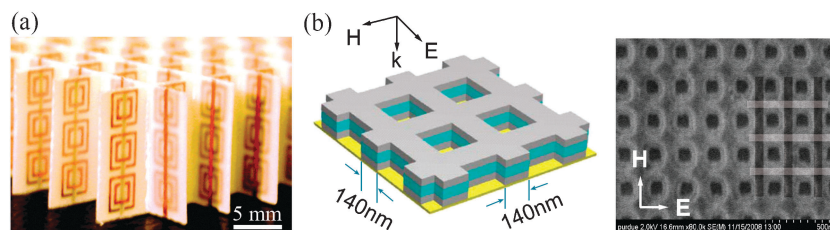


Fig. 4 (a) NIMs working at microwave frequencies, which consist of copper SRRs and wires deposited lithographically on standard circuit boards. The size of the unit cell is 5 mm. Reprinted from ref. 15 with permission. (b) Fishnet structure as NIMs in the visible region (yellow light). The left panel is the schematic of the fishnet structure, in which two layers of metal meshes (gray) are separated by a dielectric layer (cyan). The right panel is the scanning electron microscope (SEM) image of the sample fabricated by electron beam lithography (EBL). Reprinted from ref. 22 with permission.

conventional approach of combing SRRs and metallic wires. In addition, the EM waves are incident normal to the fishnet sample surface to produce the negative refractive index. This configuration is much easier than that for NIMs based on SRRs and wires, which require oblique incidence of EM waves to excite SRRs with out-of-plane magnetic fields for strong magnetic resonances.

The rapidly growing metamaterials research is driven by a number of potential applications of metamaterials. At the early stage of metamaterials research, besides magnetic resonance imaging, novel microwave circuits, and antennas at microwave region,^{23–25} perfect lens with imaging resolution beyond the diffraction limit is one of the most attractive devices.^{26,27} In conventional optical systems, we cannot resolve two points separated less than $\lambda/2n$, where n is the refractive index of the ambient medium. This fundamental limitation exists because the information of the object's fine features is carried by evanescent waves, which exponentially decay in space. All the information relevant to the subwavelength details of the object is lost, before reaching the imaging plane. However, a flat slab of NIM, proposed by Pendry, can work as a perfect lens to recover all the lost information.²⁶ This remarkable property of perfect lens arises from the fact that the initially decayed evanescent waves are now amplified through the NIM slab. Meanwhile, the propagating waves are focused due to the negative refraction and reversed phase front. As a result, a NIM slab incredibly brings both propagating and evanescent waves to a perfect focus (Fig. 5(a) and (b)), without suffering the traditional constraint imposed by the diffraction limit.

The concept of perfect lenses has been experimentally demonstrated at microwave, mid-infrared and optical frequencies with different designs.^{28–31} In ref. 30, using a silver thin film to enhance the evanescent wave under the transverse magnetic (TM) polarization condition, sub-diffraction-limited imaging with 60 nanometre half-pitch resolution, or one-sixth of the illumination wavelength was accomplished. The image of arbitrary nanostructures with sub-diffraction-limited resolution was also demonstrated based on the silver superlens. The recorded image “NANO” (middle panel of Fig. 5(c)) reproduced the fine features from the object mask (top panel of Fig. 5(c)) in all directions with good fidelity, while the image of “NANO” in the control experiment without the

superlens showed a much wider linewidth (bottom panel of Fig. 5(c)). Recently, researchers have made significant progress in this area, and have been capable of achieving subwavelength spatial resolution in the far field by converting evanescent waves into propagation waves. For more details, readers can refer to the recent review paper on this specific topic.²⁷

In addition, tunable metamaterials can be used for switching and modulating EM waves if the properties of metamaterials can be controlled. Different modulation approaches were demonstrated, including electrically/optically pumping the semiconductor constituent of the metamaterials,^{32–35} electro-control of the anisotropic optical constant of liquid crystal inclusions,^{36,37} external DC magnetic field tuning^{38,39} and the thermal effect.^{40,41} Another interesting application of metamaterials is perfect absorbers, stemming from the possibility to design metamaterial elements which can individually absorb the electric and magnetic components of incident EM waves.^{42,43}

4. Chiral metamaterials

Metamaterials can implement more sophisticated structures, such as chiral ones. The term chiral is used to describe an object that is non-superimposable on its mirror image. The literal origin of chiral is from the Greek word for hand. In fact, human hands are an excellent example of chiral objects (Fig. 6(a)). The right hand can never be superposed on the left hand, and *vice versa*, no matter how we orientate the two hands. In contrast, an object is achiral (non-chiral) if and only if it has an axis of improper rotation; that is, an n -fold rotation (rotation by $360^\circ/n$) followed by a reflection in the plane perpendicular to this axis that coincides the object with itself. In chemistry, biology and pharmaceuticals, chiral molecules are an important context. Many biologically active molecules, such as the naturally existing amino acids, enzymes and sugars, are chiral. A chiral molecule and its mirror image are called enantiomers, which are often designated as “right-handed” and “left-handed” enantiomer, respectively. Astonishingly, all naturally occurring proteins are made of left-handed amino acids. The cause of such homochirality is still under debate, but is crucial to the origins of life.

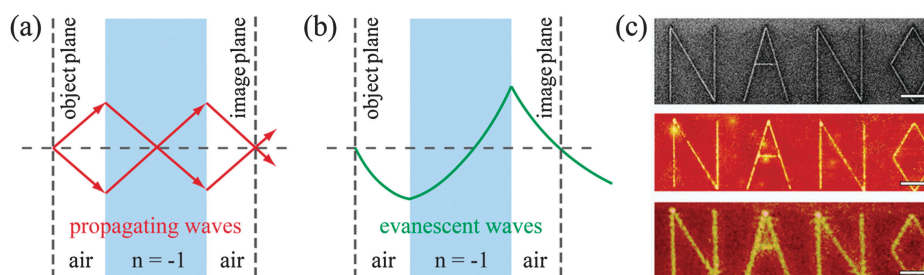


Fig. 5 (a) A flat NIM slab can focus all the light rays from a point source, arising from the negative refraction. (b) The NIM slab can also amplify evanescent waves, leading to perfect imaging at the image plane. (c) Experimental demonstration of an optical silver superlens. Top: focused ion-beam (FIB) image of the “NANO” object. The linewidth is 40 nm. Middle: atomic force microscopy (AFM) of the developed image on photoresist with a silver superlens. The linewidth is 89 nm. Bottom: AFM of the developed image without a silver superlens. The line width is 321 ± 10 nm. The scale bars indicate 2 μ m. Reprinted from ref. 30 with permission.

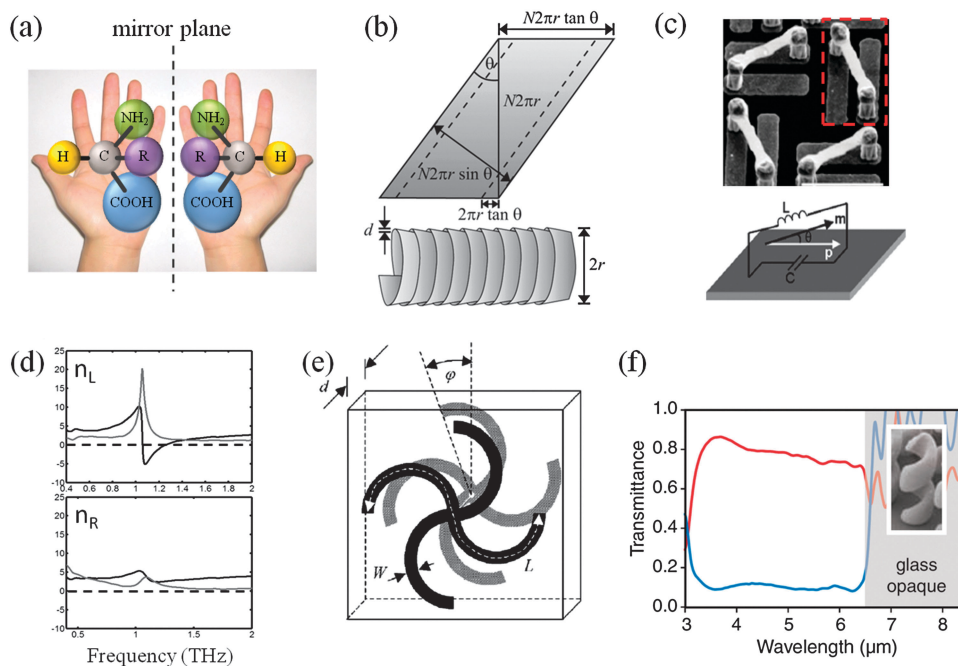


Fig. 6 (a) The left-handed and right-handed enantiomer of a generic amino acid. (b) Chiral Swiss roll structures proposed by Pendry to achieve the negative refractive index. Reprinted from ref. 46 with permission. (c) Top: SEM image of one unit cell of terahertz chiral structures. Bottom: the equivalent circuit of one chiral resonator outlined in red in the top image. Reprinted from ref. 47 with permission. (d) Experimentally retrieved effective refractive index for left- and right-handed circularly polarized light, shown in top and bottom panel, respectively. The black curve is the real part of the refractive index, while the gray one is the imaginary part. A negative refractive index exists for the left-handed circularly polarized light but not for the other polarization. Reprinted from ref. 47 with permission. (e) Left-handed enantiomeric bilayered structures constructed from planar metallic rosettes, which are separated by a dielectric slab of thickness d and twisted by an angle ϕ with respect to each other. Reprinted from ref. 55 with permission. (f) Transmittance spectra of left-handed circularly polarized light (red curve) and right-handed circularly polarized light (blue curve) through two-pitch right-handed gold helices. For wavelengths longer than $6.5 \mu\text{m}$, the glass substrate becomes totally opaque. Hence, transmittance cannot be measured. The inset shows the oblique view of right-handed helices, which are fabricated by direct laser writing into a positive-tone photoresist followed by electrochemical deposition of gold. Reprinted from ref. 61 with permission.

From the electromagnetic point of view, chiral materials satisfy the following constitutive equations:⁴⁴

$$\begin{cases} \vec{D} = \epsilon_0 \epsilon_r \vec{E} + i\kappa \sqrt{\epsilon_0 \mu_0} \vec{H} \\ \vec{B} = \mu_0 \mu_r \vec{H} - i\kappa \sqrt{\epsilon_0 \mu_0} \vec{E} \end{cases} \quad (15)$$

where κ is the dimensionless chirality parameter with a nonzero value. Apparently, different from normal isotropic materials characterized by constitutive relation of eqn (2), the electric (magnetic) induction depends on both the electric and magnetic components of the EM field. In other words, there is a cross-coupling between the electric and magnetic field in a chiral medium. It can be further proved that for left- and right-handed circularly polarized light propagating in a chiral medium, the refractive index is given by:

$$n_{L/R} = \sqrt{\epsilon_r \mu_r} \pm \kappa \quad (16)$$

This means one circular polarization will experience a slower phase velocity. If the chirality parameter κ is sufficiently large, the phase velocity, and hence the refractive index can be even negative. Based on this investigation, Tretyakov *et al.* and Pendry independently suggested that chiral materials provide an alternative route to realize the negative refractive index.^{45,46} This approach does not require simultaneously negative

permittivity and permeability in the same frequency range as we have discussed in preceding sessions, which could relax the design and fabrication challenges to some extent.

To achieve a strong chirality leading to the negative refractive index, Pendry proposed the Swiss roll structure wound in a helical manner, as shown in Fig. 6(b).⁴⁶ Similar to SRRs, the structure has resonance due to the inductance of the coiled helix and capacitance between the inner and outer layers of the helix. As current flows along the chiral Swiss roll structure, it generates not only a magnetic polarization along the axis, but also an electric polarization as part of the current flows parallel to the axis. The feature that electric polarization and magnetic polarization are parallel is consistent with what eqn (15) implies for chiral materials. Moreover, the chirality is enhanced in such artificial resonant structures.

The chiral route towards the negative refraction index inspired many research groups to work along this direction.^{47–53} In 2009, Zhang *et al.* designed and characterized a new type of terahertz chiral metamaterials.⁴⁷ The sample is composed of an array of micrometre-scale vertical gold resonators, in which the chirality is introduced by tilting the loop of the resonator out of the plane. One unit cell consists of four chiral resonators with four-fold rotational symmetry to improve the isotropy of the structure (Fig. 6(c)). The chiral resonator can be modelled as an LC resonant

circuit, whose inductor originates from the loop and the capacitor arises from two bottom metal strips. The oscillating currents flowing through the metal loop can be excited by either an electric field across the gap or a magnetic field threading through the loop, which in turn generate strong electric and magnetic responses. Since the electric and magnetic dipoles share the same structural resonance, the excitation of one dipole would inevitably lead to the excitation of the other, in accordance with the general feature of a chiral medium (see eqn (15)). Moreover, the two induced dipoles are almost parallel; therefore a strong chiral behavior is expected. Indeed, by analyzing transmission and reflectance of light at normal incidence to the chiral structure using terahertz-time-domain spectroscopy, Zhang *et al.* convincingly demonstrated that the negative refractive index exists for one circular polarization (Fig. 6(d)). Soukoulis' group experimentally studied another non-planar chiral structure,⁴⁸ which is similar to the design proposed by Marqués *et al.* in 2007.⁴⁹ The structure in ref. 48 is formed by two identical SRRs separated by a dielectric substrate and interconnected by two metallic pillars. When the structure is excited by external EM waves, both magnetic dipole and electric dipole exist and they are both parallel to the axis of the SRRs. The negative refractive index was experimentally and numerically demonstrated at the microwave wavelength.

Meanwhile, planar chiral metamaterials have been extensively investigated, since they can also exhibit strong chirality and they are relatively easier to fabricate compared to the non-planar structures. The designs include bilayered rosette,⁵⁰ cross-wire,⁵¹ and U-shaped structures.⁵² The patterns on each layer are mutually twisted by an angle, giving rise to an extremely considerable optical rotation and consequently a negative refractive index. Readers can refer to a recent review paper on chiral metamaterials for more information.⁵³

In fact, the study of chiral materials (both natural and artificial ones) has been a long history.⁵⁴ In 1813 Jean Baptiste Biot discovered that the plane of polarization of a linearly polarized light was rotated either to the right or the left, when it passed through quartz single crystals or aqueous solutions of tartaric acid or sugar. Substances that can rotate polarized light are called optically active, as they interact with light. In 1848 Louis Pasteur deduced that such an optical activity has a molecular origin, which eventually influences how macroscopic materials interact with polarized light. The first artificial composite materials displaying the analogue of optical activity but in the microwave region were introduced by J. C. Bose in 1898. Nowadays, many novel microwave devices, such as antennas, polarizers and waveguides, are based on artificial chiral materials.

With the advance of simulation and fabrication techniques, people are able to realize a variety of chiral structures to enhance the light–matter interaction. Strong optical activities have been demonstrated by planar or three-dimensional chiral metamaterials. In 2003, Zheludev's group reported the first optical manifestation of chirality in a two-dimensional (2D) planar system, which was composed of a single layer of metallic rosette structures arranged in a square lattice.⁵⁵ A large rotation of polarization more than 30° was observed experimentally. The rotation was believed to be associated with both the chirality of the structure itself and the

arrangement of the structures. Later on, several work demonstrated extremely strong polarization rotation based on various rosette structures.^{50,51,56,57} The rotary power per wavelength can be five orders of magnitudes stronger than a gyrotropic quartz crystal. Remarkably, only two layers of the artificial chiral structures, which are twisted with a small angle, are sufficient to realize such giant polarization rotation (Fig. 6(e)). Pronounced chiral behaviours such as optical activity and circular dichroism were observed in the optical region based on nanoscaled bilayered chiral structures.^{58–60} Very recently, light propagation through three-dimensional gold helices has been investigated in the mid-infrared region.⁶¹ The structure can block the circular polarization with the same handedness as the helices, while it transmits the other with very high efficiency over a broad wavelength band (Fig. 6(f)).

5. Interaction of meta-atoms

At the early stage of metamaterials research, most attention was concentrated on the effective properties of metamaterials, implying that the coupling among individual elements is somewhat ignored. Recently, the interaction of meta-atoms has become a very important subfield of metamaterials, because it not only provides better insight to the underlying mechanism of metamaterials, but also leads to numerous interesting phenomena.

In analogy to the electronic or molecular energy theory, when electric or magnetic meta-atoms interact, the energy levels of the coupled system will split from the initial isolated state. Such a simple “hybridization” model can be well applied to quantitatively analyze composite structures of greater geometrical complexity. In 2003, Halas and Nordlander group at Rice University first introduced the “hybridization” approach to electric plasmon structures.⁶² As shown in Fig. 7(a), the resonance frequencies of a metallic nanoshell structure can be considered as the result from the interaction between a nanosphere and a nanocavity. The plasmon modes of sphere and cavity induce surface charges at the interfaces of the shell. Due to the finite thickness of the nanoshell, the sphere and cavity plasmon modes are coupled with each other. This interaction gives rise to the splitting of the plasmon resonance. One is a symmetric or “bonding” plasmon mode with a lower resonance frequency ω_- , and the other one is an antisymmetric or “antibonding” mode with a higher resonance frequency ω_+ . Apparently, the coupling strength between the sphere and cavity plasmons is inversely proportional to the shell thickness. The thinner the nanoshell is, the larger is the energy splitting.

Similarly, when two magnetic artificial atoms, such as SRRs, are close to each other, the interaction between them is no longer negligible.^{63–65} The mutual inductance M between two SRRs gives rise to hybridized magnetic molecular states. Based on the Lagrangian approach, the new eigenfrequencies can be written as $\omega_{\pm} = \omega_0/\sqrt{1 \mp \xi}$. Here $\omega_0 = 1/\sqrt{LC}$ is the initial resonance frequency of uncoupled SRRs, and ξ denotes the coupling strength given by the ratio between the mutual inductance and internal inductance of SRRs ($\xi = M/L$). Again, ω_- is the resonance frequency of the symmetric bonding state in which the two SRRs oscillate in phase, while ω_+ is the

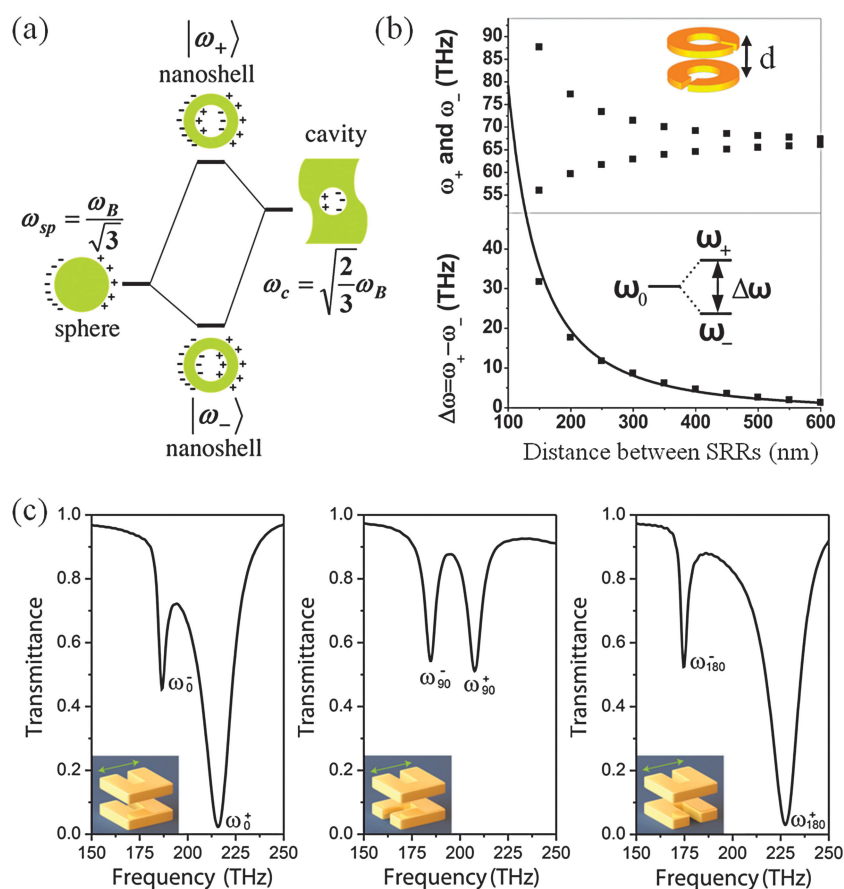


Fig. 7 (a) The energy-level diagram to describe the electric plasmon hybridization in metal nanoshells. The two resonance frequencies of nanoshells result from the interaction between the sphere and cavity plasmons. Reprinted from ref. 62 with permission. (b) Hybridization of magnetic meta-atoms. The figure plots the dependence of the resonance frequencies ω_{\pm} as well as the frequency gap $\Delta\omega = \omega_{+} - \omega_{-}$ on the separation between two SRRs. Reprinted from ref. 64 with permission. (c) Numerically simulated transmittance spectra for SRR stereometamaterials with twist angles of 0° , 90° , and 180° , respectively. Clearly, the optical properties are sensitive to the arrangement of SRRs. Reprinted from ref. 70 with permission.

resonance frequency of the antibonding state in which SRRs oscillate out of phase. Because the mutual inductance dramatically increases as reducing the separation of SRRs, a large splitting in the resonance frequency is expected. Fig. 7(b) plots the eigenfrequencies ω_{\pm} and the frequency difference $\Delta\omega = \omega_{+} - \omega_{-}$. As expected, an increase in the frequency difference $\Delta\omega$ is observed, when the distance between the two SRRs is decreased. Moreover, for arrays of SRRs, the hybridization gives rise to a quasi-continuous energy band, which have been demonstrated in the microwave and optical range.^{66–68}

SRRs exhibit not only fundamental magnetic responses, but also profound plasmon resonances inherent in metallic structures. As a result, SRRs offer an idea platform to study all possible couplings, that is, electric dipole–dipole, magnetic dipole–dipole, electric dipole–magnetic dipole, and even higher-order electric multipolar interactions. Depending on the relative orientation of the two SRRs and the polarization of external EM waves, the interplay of SRRs could be quite intricate, which alters the optical properties of coupled SRRs dramatically.⁶⁹ In chemistry, stereoisomers refer to materials whose properties depend not only on the type of atoms

comprising the materials, but also on the spatial arrangement of the atoms within the molecules. Inspired by this concept, Liu *et al.* investigated two layers of identical SRRs, but with various twist angles in each unit cell.⁷⁰ It is found that the optical properties of such metamaterials can be significantly modified by changing the mutual twist angle between the two SRRs, owing to the variation of electric and magnetic interactions (Fig. 7(c)). The feasibility to tune the resonant behaviour in the proof-of-concept system by altering the spatial arrangement of the constituent magnetic atoms suggests an alternative way to engineer more complex artificial molecules with multiple functions. For example, we can design “stereometamaterials” to control optical polarization as stereoisomers and liquid crystals do, or realize the optical properties of biomolecules such as double helix DNA proteins.

Another appealing topic associated with meta-atom interactions is electromagnetically induced transparency (EIT),⁷¹ recently investigated by several groups.^{72–80} EIT was first discovered in atomic systems. In a three-level atomic EIT system,⁷¹ the coupling between the excited energy level $|2\rangle$ with a dipole-allowed transition to the ground state $|1\rangle$ and a metastable level $|3\rangle$ by a control beam leads to a destructive

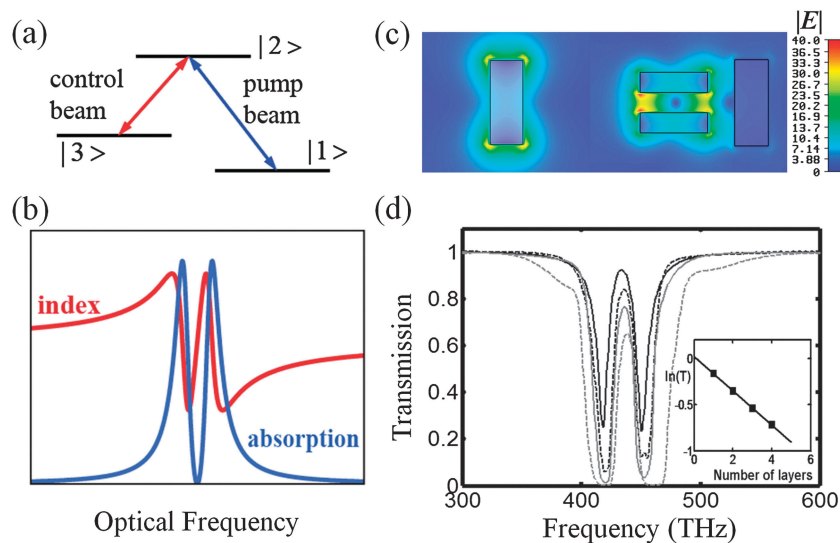


Fig. 8 (a) The scheme of a three-level atomic EIT system. (b) Rapid changes of refractive index (red curve) and absorption (blue curve) associated with atomic EIT. In the center of the transparency window, the steep, linear region of the refractive index gives rise to slow light with low losses. (c) Metamaterial-based EIT system. Left: an uncoupled bright atom. Right: a dark atom (a pair of metallic strips) coupled with a bright atom (one strip). The colour represents the field distribution at resonance. Reprinted from ref. 72 with permission. (d) The transmission spectra for one (black curve), two (black dashed curve), three (gray curve), and four (gray dashed curve) layers of periodic EIT molecules. The inset shows the natural logarithm of peak transmission *versus* the number of layers along the propagation direction at the transparency frequency. Reprinted from ref. 72 with permission.

interference (Fig. 8(a)). This destructive interference can render a transparent window within a broad absorption band (Fig. 8(b)). A meta-molecule consisting of one radiative or bright mode (*e.g.*, electric dipole) and one subradiative or dark mode (*e.g.*, magnetic dipole, or electric quadrupole) can mimic an atomic EIT system. As discussed in ref. 72, a metal strip functions as an optical dipole antenna. Hence it serves as the bright atom in the meta-molecule. Next to the bright atom, a pair of metal strips with slightly smaller dimensions is introduced. Due to the hybridization, the strip pair has symmetric and antisymmetric modes. The antisymmetric mode has counter-propagating currents on the two strips. Consequently, it can be regarded as a dark mode without direct electrical dipole coupling with the radiation fields. By carefully designing the strip geometries, the central resonance frequencies of the bright atom and the dark atom can be overlapped. When the two structures are placed side by side (Fig. 8(c)), EIT-like destructive interference happens between two pathways: direct dipole excitation of the bright atom from the incident wave and excitation of the dark atom (by the bright atom) coupling back to the bright atom. A small spectral window of transparency in the broad absorption band is observed in the simulation (Fig. 8(d)), and confirmed experimentally in a slightly different configuration based on a stacked metamaterial.⁷⁶ These results promise a variety of potential applications. First, low-loss optical metamaterials could be realized, benefitting from the significantly suppressed radiative losses. Second, the highly dispersive (phase) refractive index around the EIT resonance frequency implies a large group index. Therefore, we could construct compact slow-light devices based on nanoscale metamaterial structures. Finally, the sharp spectral resonance can facilitate biochemical detection with high sensitivity.⁷⁷

6. Transformation optics

In optics, Fermat's principle states that light, travelling between two points, will follow the route with the smallest optical path length. Snell's law and the law of reflection in fact result directly from this principle. In the space where light propagates, if we replace one material with another one with a different refractive index, the light path will be altered according to Fermat's principle. The goal of transformation optics is to precisely control the flow of light in desirable manners, by spatially tailoring the material property. With the aid of the full range of available effective permittivity and permeability provided by metamaterials, people have been able to realize many exotic optical phenomena and devices, including invisible cloaks, illusion optics, optical black holes, beam shifters, field rotators, light concentrators, lossless waveguide bends and many more.^{81,82}

We first take the invisible cloak as an example to elaborate the basic concept of transformation optics,^{83–87} as illustrated in Fig. 9(a). Suppose we pull and stretch the space to open a circular void ($r < R_1$). The initial uniform light rays are then partially squeezed into a shell ($R_1 < r < R_2$), while the remaining light rays (in the region $r > R_2$) are maintained. Waves cannot penetrate into and hence interact with the core region, because it is not part of the transformed space. No matter what objects are placed inside the core, it is perceived to an observer that nothing exists; that is, the object is concealed or cloaked. The distortion of space can be tracked by certain coordinate transformations. Meanwhile, the form invariance of Maxwell's equations implies that the coordinate transformation can instead be applied to the permittivity and permeability, giving rise to the prescription of the spatial profile of the material property that enables us to achieve

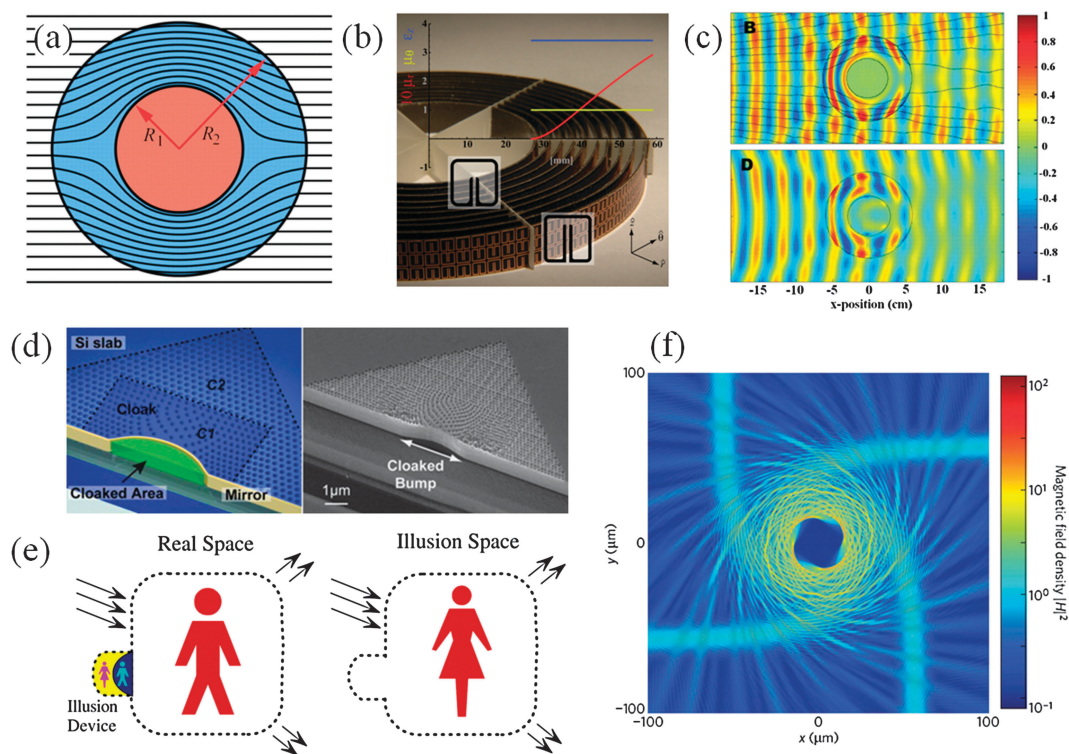


Fig. 9 (a) Schematic of a cloak in a two-dimensional view, reprinted from ref. 83 with permission. The rays, representing the Poynting vector, divert within the annulus of the cloak region ($R_1 < r < R_2$), while emerge on the far side without any scattering and distortion. (b) Image of a 2D microwave cloak made of SRRs, reprinted from ref. 85 with permission. The background plots the values of prescribed material properties. (c) Simulated (top) and experimentally mapped (bottom) field patterns of the cloak. Reprinted from ref. 85 with permission. (d) Schematic (left) and SEM image of an optical carpet cloak, by drilling holes in a Si slab. Reprinted from ref. 91 with permission. (e) Schematic of illusion optics. An illusion device is placed next to an object (a man) which transforms it into the illusion image (a woman). Reprinted from ref. 102 with permission. (f) Simulated field distribution of light travelling through a dense optical medium. A photon trap absorbs light from all directions, mimicking the black hole phenomenon. Reprinted from ref. 103 with permission.

the desired light flow.^{81–84,88} The resulting medium is normally highly anisotropic and spatially complex. The first proof-of-principle cloak is built by ten cylindrical layers of SRRs working over a band of microwave frequencies.⁸⁵ The SRRs have different geometrical parameters (Fig. 9(b)), therefore realizing the predesigned spatial distribution of anisotropic permittivity and permeability. The experimental results showed that the cloak could significantly decrease scattering from the hidden object and also reduce its shadow. From Fig. 9(c), one can visualize how smoothly the waves wrap around the core and propagate to the far side with less perturbed phase front.

The early cloak devices usually require extreme values for the metamaterial properties, resulting in disadvantages of narrow operation band and high loss. A number of new designs are proposed to mitigate these constraints.^{89–95} In particular, the carpet cloak can significantly relax the variation range of the material properties,^{89–92} since the carpet cloak compresses the curved surface in only one direction into a conducting sheet and hence a quasi-conformal mapping technique can be applied to the two-dimensional system. Any arbitrarily shaped object placed behind the curved bump will maintain the reflectance of a smooth, flat surface, rendering the object invisible. Recently, the major step towards optical cloak based on this scheme has been experimentally

demonstrated. One of the cloak devices is formed by etching holes in a silicon slab (Fig. 9(d)). Holes are spatially distributed to realize the gradient index profile calculated from the conformal mapping method. The good performance of the cloak is confirmed over a broad wavelength range from 1400 to 1800 nm. The reported carpet cloak is isotropic and non-resonant, strongly implying the feasibility to design a new class of broadband and low-loss optical devices based on transformation optics. Subsequently, Ergin *et al.* designed and realized a quasi 3D carpet cloak operating at the optical wavelengths, which was based on a dielectric woodpile photonic crystal.⁹⁶ Another research group presented a 3D carpet cloak with a rotational symmetry, albeit operating at microwave frequencies.⁹⁷ Very recently, transformation optics has been applied to surface plasmon polaritons, bound surface waves at the metal–dielectric interface.^{98–101} The invisibility cloak, waveguide bend, and concentrator for surface plasmon polaritons have been successfully demonstrated, opening up a new avenue for manipulating near-field optical waves.

Transformation optics can play more tricks. In addition to cloaking an object, transformation optics can also create a stereoscopic illusion, making an arbitrary object appear like another object with a completely different shape. Lai *et al.* first numerically demonstrate this unusual optical phenomenon.¹⁰² The key of an illusion device lies in two distinct pieces of

metamaterials, termed the “complementary medium” and the “restoring medium” by the authors. As schematically shown in Fig. 9(e), the complementary medium annihilates the adjacent space and cancels any light scattering from an object itself (a man in the figure). Then the restoring medium recovers the cancelled space with a new illusion space that embraces another object chosen for the illusion (for example, a woman). Regardless of the beam profile and the incident direction of the light, the illusion device can always create a stereoscopic illusion for any external observers. More interestingly, the illusion device can work at a distance from the object. It is shown that this “remote” feature enables us to open a virtual aperture in a wall so that one can peep through the wall.

Transformation optics allows us to bend light in space in nearly arbitrary manners, similar to general relativity where time and space are curved. In the general relativity, the presence of gravitational fields results in the motion of matter and the light propagating in a curved space–time domain. This behaviour can be mimicked by light propagation in a space filled with inhomogeneous metamaterials. Indeed, researchers have been moving forward to extend the analog, so that light propagation through gradient-index metamaterials can be used as a laboratory platform to investigate some astronomic phenomena, including celestial orbitals and black holes.^{103–105} It is shown theoretically that a continuous-index photon trap could serve as the black hole, absorbing light in all directions over a broad frequency band with high efficiency (Fig. 9(f)).¹⁰³ Such a photonic black hole could be formed by mixing air and high-index semiconductor indium gallium arsenide phosphide (InGaAsP), which would attract light in the same way a gravitational black hole attracts matter and light. Independently, Narimanov and Kildishev at Purdue University theoretically proposed a similar idea based on transformation optics.¹⁰⁴ They envision that the photon black holes could be applied to photovoltaics, solar-energy harvesting, and optoelectronic detectors. A recent experimental work reports the electromagnetic black hole made of non-magnetic metamaterials, which can omnidirectionally absorb light over a broad band in the microwave region.¹⁰⁵

7. Future directions

Considering the fundamental research and application purposes, it is highly desirable to have truly bulk metamaterials, which are on the scale of tens of wavelengths, or even larger in all three dimensions. 3D metamaterials can be realized by focused ion beam milling through metal–dielectric multilayers (for example, the fishnet structure),¹⁰⁶ or combining advanced planar micro-/nano-manufacturing techniques (such as optical lithography¹⁰⁷ and electron beam lithography⁶⁸) for individual layers with sophisticated alignment procedures to stack different layers. Meanwhile, direct laser writing by multiphoton polymerization of a photoresist¹⁰⁸ has emerged as a technique for the flexible fabrication of 3D metamaterials.^{61,96} This method utilizes a multi-photon absorption process in a photoresist that is transparent at the wavelength of the laser used for creating the pattern. If the laser beam is tightly focused into the photoresist, the light intensity becomes sufficiently high to induce the multiphoton absorption and

hence the polymerization process. By properly scanning and modulating the laser, an arbitrary three-dimensional connected pattern, either periodic or non-periodic, can be created.

However, using the aforementioned top-down techniques, it is extremely difficult and time-consuming to realize bulk optical metamaterials, because we need to precisely control the feature size and spacing of metamaterials at the nanoscale over a large domain, and the fabrication process is usually non-parallel. The bottom-up and self-assembly techniques may promise solutions to these fabrication challenges. For example, all-angle optical negative refraction, arising from the hyperbolic constant frequency contour of one unique indefinite metamaterial,^{109–113} has been experimentally demonstrated in metallic nanowire metamaterials with thickness about ten times of the wavelength (Fig. 10(b)). This structure is fabricated by electrochemically growing metallic nanowires in a porous alumina template, which is prepared by the anodization method in a self-organized way.¹¹⁴ Such a method has proved to be a low-cost and high-yield technique for fabricating different kinds of nanostructures including nanowires, nanodots and nanotubes.^{115,116} In addition, it has been shown that clusters of metallic nanoparticles exhibit pronounced electric and magnetic responses, which may be good candidates of building blocks for constructing optical NIMs (Fig. 10(c)).^{117–119} With recent advances in particle self-assembly techniques, it is possible to form the prescribed particle colloids, by tailoring the shape-dependent capillary interactions and surface energies to control the particle orientation and spatial arrangement in three dimensions.^{120,121} Ultimately, some atomic, molecular, and condensed matter systems may be used to realize metamaterials. It has been shown that quantum interference effects similar to EIT can lead to a large induced chirality under realistic conditions, which enable negative refraction with minimal absorption.¹²² In addition, based on a two-component system in which one atomic or molecular component may be inverted, the authors of ref. 123 predict the existence of nonmagnetic amorphous solids and liquids that have a negative refractive index.

Nonlinear metamaterials, whose properties depend on the intensity of EM waves, is an emerging area worth extensive investigation especially in the optical regime. In the seminal paper, Pendry *et al.* already predicted the enhanced nonlinear optical properties by inserting nonlinear elements into the gap of SRRs, arising from the giant local-field amplification.⁸ Subsequently, theoretical work has predicted that nonlinear metamaterials could offer novel phenomena such as hysteretic transition,¹²⁴ unusual wave mixing¹²⁵ and solitary wave propagation.^{126,127} One particular interesting phenomenon is the reversed Manley–Rowe relation and backward phase-matching condition for second-harmonic generation (SHG) or optical parametric amplification (OPA).¹²⁸ Suppose a metamaterial has a negative refractive index at the fundamental frequency ω_1 and a positive refractive index at the second-harmonic frequency ω_2 . At ω_1 the energy flow (Poynting vector) points from left to right, for example; then the wave vector \vec{k}_1 must point from right to left arising from NIMs at ω_1 . The phase matching condition, *i.e.*, $\vec{k}_2 = 2\vec{k}_1$, requires that the wave vector \vec{k}_2 at the second harmonic frequency ω_2 also travels from the right to the left. Since the

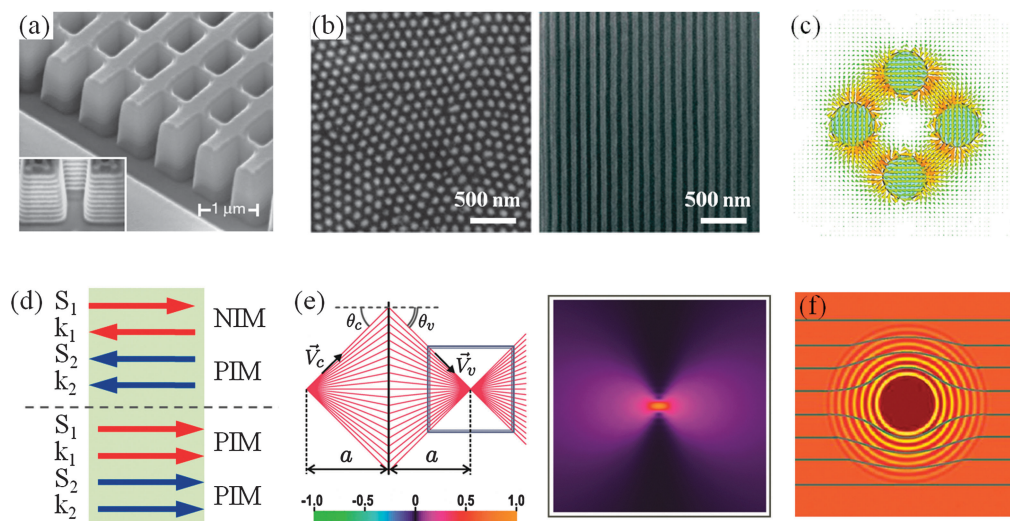


Fig. 10 (a) A 3D fishnet NIM structure fabricated by the top-down method (FIB), which consists of 21 total layers of alternating silver (30 nm) and MgF_2 (50 nm) films. The inset shows the cross-section view. Reprinted from ref. 106 with permission. (b) Silver nanowire metamaterials fabricated by the bottom-up technique. Left and right SEM images show the top and cross-section view, respectively. Reprinted from ref. 114 with permission. (c) Magnetic resonators composed of four metallic nanospheres. Reprinted from ref. 117 with permission. The structure may be synthesized from the self-assembly method. (d) Schematic of SHG when NIMs are involved, in comparison with normal SHG in only PIMs. (e) Focusing of electrons by a grapheme p-n junction. The left panel plots the trajectories of electrons, diverging from a source at the distance a from the junction and becoming convergent after negative refraction. The right panel shows the interference-induced pattern in the charge current near the focal image. Reprinted from ref. 133 with permission. (f) A matter-wave cloaking system involves cold atoms within a three-dimensional laser-based optical lattice. Matter waves travelling through the medium bend around the atoms inside as though they are not there.

metamaterial possesses a positive refractive index at ω_2 , the energy flow is at the same direction with the wave vector. As a result, the second harmonic signal is maximal at the incident interface rather than the exit interface of the metamaterial slab, in sharp contrast to SHG in normal dielectric materials (see the comparison in Fig. 10(d)). Such extraordinary phenomenon could be demonstrated in currently available metamaterials, such as the 3D fishnet structures shown in Fig. 10(a), at proper frequencies. Moreover, artificial magnetic metamaterials could provide additional routes to boost the nonlinear process.¹²⁹ In terms of applications, tunable metamaterials^{130,131} and memory devices¹³² have been experimentally demonstrated based on nonlinear metamaterials.

Finally, metamaterials may manifest fascinating phenomenon in the quantum world. In principle, the concept of metamaterials could be applied to any wave at any scale, including the matter wave which is the wave description of particles, such as electrons and neutrons, in quantum mechanics. Indeed, researchers have taken theoretical efforts towards this direction. Cheianov *et al.* theoretically demonstrated that negative refraction and focusing of electrons can be achieved in grapheme (Fig. 10(e)), a monolayer of graphite.¹³³ From solid state physics, we know that electrons in the valence (conduction) band have a group velocity antiparallel (parallel) to the wave vector. This provides a delicate connection with optical negative refraction, which requires group and phase velocities of light opposite in signs. By examining a grapheme p-n junction, Cheianov *et al.* numerically show that a point source of electron current in the n-type region radiates electrons to the interface, where they are negatively refracted into the p-type region and brought to a focus. This is just in analogy to light focused by an NIM slab.

Moving forward, using time-invariant coordinate transformations of Schrödinger's equations, Zhang *et al.* have recently designed an invisibility cloak for matter waves.¹³⁴ The new type of cloaks is a three-dimensional optical lattice of laser beams, consisting of optical standing waves with gradually varying amplitude along the radial direction. The varying amplitude of the optical lattice changes the effective mass and band energy of the hidden object as another atom or wave moves near it, causing the stream of particles or incident matter waves to bend and come out on the other side of the object as if it was not there (see Fig. 10(f)). Other proposals bridging metamaterials with quantum mechanics include modifying the emission rate of an emitter adjacent to carefully designed metamaterials with large photon densities of state,^{135,136} as well as exploring the possibility of repulsive Casimir forces that originate from the quantum zero-point oscillation of EM waves.^{137–142}

8. Conclusions

Without any doubt, metamaterials have become an extremely exciting research area. The unique electromagnetic properties provided by metamaterials attract considerable attention of researchers from multiple disciplines. In turn, this will spark the merging of knowledge and expertise across different areas, further driving the astounding advance of metamaterials research. Within only ten years, we have witnessed many remarkable breakthroughs, such as negative refraction, superlens and invisible cloak. Many other fascinating discoveries and applications are waiting for us to explore. With the complete degree of freedom to control over material properties, what we could do next is only limited by our imagination.

Acknowledgements

The authors are grateful for the financial support from the NSF Nano-scale Science and Engineering Center (NSEC) under grant number CMMI-0751621.

References

- D. R. Smith, J. B. Pendry and M. C. K. Wiltshire, *Science*, 2004, **305**, 788–792.
- S. A. Ramakrishna, *Rep. Prog. Phys.*, 2005, **68**, 449–521.
- L. Fok, M. Ambati and X. Zhang, *MRS Bull.*, 2008, **8**, 3998–4001.
- N. Fang, D. J. Xi, J. Y. Xu, M. Ambati, W. Srituravanich, C. Sun and X. Zhang, *Nat. Mater.*, 2006, **5**, 452–456.
- J. D. Jackson, *Classical Electromagnetism*, John Wiley & Sons, New York, 3rd edn, 1999.
- V. G. Veselago, *Sov. Phys. Usp. (Engl. Transl.)*, 1968, **10**, 509–514.
- J. B. Pendry, A. J. Holden, W. J. Stewart and I. Youngs, *Phys. Rev. Lett.*, 1996, **76**, 4773–4776.
- J. B. Pendry, A. J. Holden, D. J. Robbins and W. J. Stewart, *IEEE Trans. Microwave Theory Tech.*, 1999, **47**, 2075–2084.
- L. D. Landau, E. M. Lifshitz and L. P. Pitaevskii, *Electrodynamics of Continuous Media*, Pergamon, New York, 2nd edn, 1984.
- D. R. Smith, S. Schultz, P. Markos and C. M. Soukoulis, *Phys. Rev. B: Condens. Matter*, 2002, **65**, 195104.
- X. D. Chen, B. I. Wu, J. A. Kong and T. M. Grzegorzczak, *Phys. Rev. E: Stat. Phys., Plasmas, Fluids, Relat. Interdiscip. Top.*, 2005, **71**, 046610.
- D. R. Smith, D. C. Vier, Th. Koschny and C. M. Soukoulis, *Phys. Rev. E: Stat. Phys., Plasmas, Fluids, Relat. Interdiscip. Top.*, 2005, **71**, 036617.
- C. Menzel, T. Paul, C. Rockstuhl, T. Pertsch, S. Tretyakov and F. Lederer, *Phys. Rev. B: Condens. Matter*, 2010, **81**, 035320.
- D. R. Smith, W. J. Padilla, D. C. Vier, S. C. Nemat-Nasser and S. Schultz, *Phys. Rev. Lett.*, 2000, **84**, 4184–4187.
- R. A. Shelby, D. R. Smith and S. Schultz, *Science*, 2001, **292**, 77–79.
- T. J. Yen, W. J. Padilla, N. Fang, D. C. Vier, D. R. Smith, J. B. Pendry, D. N. Basov and X. Zhang, *Science*, 2004, **303**, 1494–1496.
- S. Linden, C. Enkrich, M. Wegener, J. Zhou, T. Koschny and C. M. Soukoulis, *Science*, 2004, **306**, 1351–1353.
- C. M. Soukoulis, S. Linden and M. Wegener, *Science*, 2007, **315**, 47–49.
- J. Zhou, T. Koschny, M. Kafesaki, E. N. Economou, J. P. Pendry and C. M. Soukoulis, *Phys. Rev. Lett.*, 2005, **95**, 223902.
- S. Zhang, W. J. Fan, N. C. Panoiu, K. J. Malloy, R. M. Osgood and S. R. J. Brueck, *Phys. Rev. Lett.*, 2005, **95**, 137404.
- G. Dolling, C. Enkrich, M. Wegener, C. M. Soukoulis and S. Linden, *Science*, 2006, **312**, 892–894.
- S. M. Xiao, U. K. Chettiar, A. V. Kildishev, V. P. Drachev and V. M. Shalaev, *Opt. Lett.*, 2009, **34**, 3478–3480.
- M. C. K. Wiltshire, J. B. Pendry, I. R. Young, D. J. Larkman, D. J. Gilderdale and J. V. Hajnal, *Science*, 2001, **291**, 849–851.
- C. Caloz, A. Sanada and T. Itoh, *IEEE Trans. Microwave Theory Tech.*, 2004, **52**, 980–992.
- A. Kurs, A. Karalis, R. Moffatt, J. D. Joannopoulos, P. Fisher and M. Soljacic, *Science*, 2007, **317**, 83–86.
- J. B. Pendry, *Phys. Rev. Lett.*, 2000, **85**, 3966–3969.
- X. Zhang and Z. W. Liu, *Nat. Mater.*, 2008, **7**, 435–441.
- A. Grbic and G. V. Eleftheriades, *Phys. Rev. Lett.*, 2004, **92**, 117403.
- A. N. Lagarkov and V. N. Kissel, *Phys. Rev. Lett.*, 2004, **92**, 077401.
- N. Fang, H. Lee, C. Sun and X. Zhang, *Science*, 2005, **308**, 534–537.
- T. Taubner, D. Korobkin, Y. Urzhumov, G. Shvets and R. Hillenbrand, *Science*, 2006, **313**, 1595.
- H. T. Chen, W. J. Padilla, J. M. O. Zide, A. C. Gossard, A. J. Taylor and R. D. Averitt, *Nature*, 2006, **444**, 597–600.
- A. Degiron, J. J. Mock and D. R. Smith, *Opt. Express*, 2007, **15**, 1115–1127.
- H. T. Chen, J. F. O'Hara, A. K. Azad, A. J. Taylor, R. D. Averitt, D. B. Shrekenhamer and W. J. Padilla, *Nat. Photonics*, 2008, **2**, 295–298.
- D. J. Cho, W. Wu, E. Ponizovskaya, P. Chaturvedi, A. M. Bratkovsky, S. Y. Wang, X. Zhang, F. Wang and Y. R. Shen, *Opt. Express*, 2009, **17**, 17652–17657.
- I. C. Khoo, D. H. Werner, X. Liang, A. Diaz and B. Weiner, *Opt. Lett.*, 2005, **31**, 2592–2594.
- Q. Zhao, L. Kang, B. Du, B. Li, J. Zhou, H. Tang, X. Liang and B. Z. Zhang, *Appl. Phys. Lett.*, 2007, **90**, 011112.
- H. J. Zhao, J. Zhou, Q. Zhao, B. Li, L. Kang and Y. Bai, *Appl. Phys. Lett.*, 2007, **91**, 131107.
- Y. Gao, J. P. Huang, Y. M. Liu, L. Gao, K. W. Yu and X. Zhang, *Phys. Rev. Lett.*, 2010, **104**, 034501.
- H. Nemeč, P. Kuzel, F. Kadlec, C. Kadlec, R. Yahiaoui and P. Mounaix, *Phys. Rev. B: Condens. Matter*, 2009, **79**, 241108.
- W. X. Huang, X. G. Yin, C. P. Huang, Q. J. Wang, T. F. Miao and Y. Y. Zhu, *Appl. Phys. Lett.*, 2010, **96**, 261908.
- N. I. Landy, S. Sajuyigbe, J. J. Mock, D. R. Smith and W. J. Padilla, *Phys. Rev. Lett.*, 2008, **100**, 207402.
- Y. Avitzour, Y. A. Urzhumov and G. Shevts, *Phys. Rev. B: Condens. Matter*, 2009, **79**, 045131.
- I. V. Lindell, A. H. Sihvola, S. A. Tretyakov and A. J. Viitanen, *Electromagnetic Waves in Chiral and Bi-isotropic Media*, Artech House Publishers, Boston, MA, 1994.
- S. Tretyakov, I. Nefedov, A. Sihvola, S. Maslovski and C. Simovski, *J. Electromagn. Waves Appl.*, 2003, **17**, 695–706.
- J. B. Pendry, *Science*, 2004, **306**, 1353–1355.
- S. Zhang, Y. S. Park, J. Li, X. C. Lu, W. L. Zhang and X. Zhang, *Phys. Rev. Lett.*, 2009, **102**, 023901.
- B. Wang, J. Zhou, T. Koschny and C. M. Soukoulis, *Appl. Phys. Lett.*, 2009, **94**, 151112.
- R. Marqués, L. Jelinek and F. Mesa, *Microwave Opt. Technol. Lett.*, 2007, **49**, 2606–2609.
- E. Plum, J. Zhou, J. Dong, V. A. Fedotov, T. Koschny, C. M. Soukoulis and N. I. Zheludev, *Phys. Rev. B: Condens. Matter*, 2009, **79**, 035407.
- J. Zhou, J. Dong, B. Wang, T. Koschny, M. Kafesaki and C. M. Soukoulis, *Phys. Rev. B: Condens. Matter*, 2009, **79**, 121104.
- X. Xiong, W. H. Sun, Y. J. Bao, M. Wang, R. W. Peng, C. Sun, X. Lu, J. Shao, Z. F. Li and N. B. Ming, *Phys. Rev. B: Condens. Matter*, 2010, **81**, 075119.
- B. N. Wang, J. F. Zhou, T. Koschny, M. Kafesaki and C. M. Soukoulis, *J. Opt. A: Pure Appl. Opt.*, 2009, **11**, 114003.
- A. Lakhtakia, *Selected Papers on Natural Optical Activity*, SPIE Milestone Volume 15, SPIE, 1990.
- A. Papakostas, A. Potts, D. M. Bagnall, S. L. Prosvirnin, H. J. Coles and N. I. Zheludev, *Phys. Rev. Lett.*, 2003, **90**, 107404.
- A. V. Rogacheva, V. A. Fedotov, A. S. Schwanecke and N. I. Zheludev, *Phys. Rev. Lett.*, 2006, **97**, 177401.
- M. Kuwata-Gonokami, N. Saito, Y. Ino, M. Kauranen, K. Jefimovs, T. Vallius, J. Turunen and Y. Svirko, *Phys. Rev. Lett.*, 2005, **95**, 227401.
- M. Decker, M. W. Klein, M. Wegener and S. Linden, *Opt. Lett.*, 2007, **32**, 856–858.
- M. Decker, M. Ruther, C. E. Kriegler, J. Zhou, C. M. Soukoulis, S. Linden and M. Wegener, *Opt. Lett.*, 2009, **34**, 2501–2503.
- M. Decker, R. Zhao, C. M. Soukoulis, S. Linden and M. Wegener, *Opt. Lett.*, 2010, **35**, 1593–1595.
- J. K. Gansel, M. Thiel, M. S. Rill, M. Decker, K. Bade, V. Saile, V. F. Georg, S. Stefan and M. Wegener, *Science*, 2009, **325**, 1513–1515.
- E. Prodan, C. Radloff, N. J. Halas and P. Nordlander, *Science*, 2003, **302**, 419–422.
- H. Liu, Y. M. Liu, T. Li, S. M. Wang, S. N. Zhu and X. Zhang, *Phys. Status Solidi B*, 2009, **246**, 1347–1406.
- H. Liu, D. A. Genov, D. M. Wu, Y. M. Liu, Z. W. Liu, C. Sun, S. N. Zhu and X. Zhang, *Phys. Rev. B: Condens. Matter*, 2007, **76**, 073101.
- D. A. Powell, M. Lapine, M. V. Gorkunov, I. V. Shadrivov and Y. S. Kivshar, *Phys. Rev. B: Condens. Matter*, 2010, **86**, 155128.

- 66 E. Shamonina, V. Kalinin, K. H. Ringhofer and L. Solymar, *J. Appl. Phys.*, 2002, **92**, 6252–6261.
- 67 G. Dolling, M. Wegener, A. Schadle, S. Burger and S. Linden, *Appl. Phys. Lett.*, 2006, **89**, 231118.
- 68 N. Liu, H. C. Guo, L. W. Fu, S. Kaiser, H. Schweizer and H. Giessen, *Nat. Mater.*, 2008, **7**, 31–37.
- 69 C. W. Chang, M. Liu, S. Nam, S. Zhang, Y. M. Liu, G. Bartal and X. Zhang, *Phys. Rev. Lett.*, 2010, **105**, 235501.
- 70 N. Liu, H. Liu, S. N. Zhu and H. Giessen, *Nat. Photonics*, 2009, **3**, 157–162.
- 71 M. Fleischhauer, A. Imamoglu and J. P. Marangos, *Rev. Mod. Phys.*, 2005, **77**, 633–673.
- 72 S. Zhang, D. A. Genov, Y. Wang, M. Liu and X. Zhang, *Phys. Rev. Lett.*, 2008, **101**, 047401.
- 73 N. Papanikolaou, V. A. Fedotov, N. I. Zheludev and S. L. Prosvirnin, *Phys. Rev. Lett.*, 2008, **101**, 253903.
- 74 P. Tassin, L. Zhang, T. Koschny, E. N. Economou and C. M. Soukoulis, *Opt. Express*, 2009, **17**, 5595–5605.
- 75 P. Tassin, L. Zhang, T. Koschny, E. N. Economou and C. M. Soukoulis, *Phys. Rev. Lett.*, 2008, **102**, 053901.
- 76 N. Liu, L. Langguth, T. Weiss, J. Kastel, M. Fleischhauer, T. Pfau and G. Giessen, *Nat. Mater.*, 2009, **8**, 758–762.
- 77 N. Liu, T. Weiss, M. Mesch, L. Langguth, U. Eigenthaler, M. Hirscher, C. Sönnichsen and H. Giessen, *Nano Lett.*, 2009, **10**, 1103–1107.
- 78 S. Y. Chiam, R. Singh, C. Rockstuhl, F. Lederer, W. L. Zhang and A. A. Bettiol, *Phys. Rev. B: Condens. Matter*, 2009, **80**, 153103.
- 79 R. D. Kekatpure, E. S. Barnard, W. S. Cai and M. L. Brongersma, *Phys. Rev. Lett.*, 2010, **104**, 243902.
- 80 L. Zhang, P. Tassin, T. Koschny, C. Kurter, S. M. Anlage and C. M. Soukoulis, 2010, <http://arxiv.org/abs/1010.2976>.
- 81 V. M. Shalaev, *Science*, 2008, **322**, 384–386.
- 82 H. Y. Chen, C. T. Chan and P. Sheng, *Nat. Mater.*, 2010, **9**, 387–396.
- 83 J. B. Pendry, D. Schurig and D. R. Smith, *Science*, 2006, **312**, 1780–1782.
- 84 U. Leonhardt, *Science*, 2006, **312**, 1777–1780.
- 85 D. Schurig, J. J. Mock, B. J. Justice, S. A. Cummer, J. B. Pendry, A. F. Starr and D. R. Smith, *Science*, 2006, **314**, 977–980.
- 86 W. S. Cai, U. K. Chettiar, A. V. Kildishev and V. M. Shalaev, *Nat. Photonics*, 2007, **1**, 224–227.
- 87 U. Leonhardt and T. Tyc, *Science*, 2009, **323**, 110–112.
- 88 G. W. Milton, M. Briane and J. R. Willis, *New J. Phys.*, 2006, **8**, 248.
- 89 J. Li and J. B. Pendry, Hiding under the Carpet: A New Strategy for Cloaking, *Phys. Rev. Lett.*, 2008, **101**, 203901.
- 90 R. Liu, C. Ji, J. J. Mock, J. Y. Chin, T. J. Cui and D. R. Smith, *Science*, 2009, **323**, 366–369.
- 91 J. Valentine, J. Li, T. Zentgraf, G. Bartal and X. Zhang, *Nat. Mater.*, 2009, **7**, 568–571.
- 92 L. H. Gabrielli, J. Cardenas, C. B. Poitras and M. Lipson, *Nat. Photonics*, 2009, **3**, 461–463.
- 93 B. Edwards, A. Alu, M. G. Silveirinha and N. Engheta, *Phys. Rev. Lett.*, 2009, **103**, 153901.
- 94 I. I. Smolyaninov, V. N. Smolyaninova, A. V. Kildishev and V. M. Shalaev, *Phys. Rev. Lett.*, 2009, **102**, 213901.
- 95 T. Zentgraf, J. Valentine, N. Tapia, J. Li and X. Zhang, *Adv. Mater.*, 2010, **22**, 2561–2564.
- 96 T. Ergin, N. Stenger, P. Brenner, J. B. Pendry and M. Wegener, *Science*, 2010, **328**, 337–339.
- 97 H. F. Ma and T. J. Cui, *Nat. Commun.*, 2010, **1**, 1–6.
- 98 P. A. Huidobro, M. L. Nesterov, L. Martín-Moreno and F. J. García-Vidal, *Nano Lett.*, 2010, **10**, 1985–1990.
- 99 Y. M. Liu, T. Zentgraf, G. Bartal and X. Zhang, *Nano Lett.*, 2010, **10**, 1991–1997.
- 100 A. Aubry, D. Y. Lei, A. I. Fernández-Domínguez, Y. Sonnefraud, S. A. Maier and J. B. Pendry, *Nano Lett.*, 2010, **10**, 2574–2579.
- 101 J. Renger, M. Kadic, G. Dupont, S. S. Aćimović, S. Guenneau, R. Quidant and S. Enoch, *Opt. Express*, 2010, **18**, 15757–15768.
- 102 Y. Lai, J. Ng, H. Y. Chen, D. Z. Han, J. J. Xiao, Z. Q. Zhang and C. T. Chan, *Phys. Rev. Lett.*, 2009, **102**, 253902.
- 103 D. A. Genov, S. Zhang and X. Zhang, *Nat. Phys.*, 2009, **5**, 687–692.
- 104 E. E. Narimanov and A. V. Kildishev, *Appl. Phys. Lett.*, 2009, **95**, 041106.
- 105 Q. Cheng, T. J. Cui, W. X. Jiang and B. G. Cai, *New J. Phys.*, 2010, **12**, 063006.
- 106 J. Valentine, S. Zhang, T. Zentgraf, U. A. Erick, D. A. Genov, G. Bartal and X. Zhang, *Nature*, 2008, **455**, 376–379.
- 107 N. Katsarakis, G. Konstantinidis, A. Kostopoulos, R. S. Penciu, T. F. Gundogdu, M. Kafesaki, E. N. Economou, T. Koschny and C. M. Soukoulis, *Opt. Lett.*, 2005, **30**, 1348–1250.
- 108 S. Kawata, H. B. Sun, T. Tanaka and K. Takada, *Nature*, 2001, **412**, 697–698.
- 109 P. A. Belov, *Microwave Opt. Technol. Lett.*, 2003, **37**, 259–263.
- 110 D. R. Smith and D. Schurig, *Phys. Rev. Lett.*, 2003, **90**, 077405.
- 111 A. J. Hoffman, L. Alekseyev, S. S. Howard, K. J. Franz, D. Wasserman, V. A. Podolskiy, E. E. Narimanov, D. L. Sivo and C. Gmachl, *Nat. Mater.*, 2007, **6**, 946–950.
- 112 Y. M. Liu, G. Bartal and X. Zhang, *Opt. Express*, 2008, **16**, 15439–15448.
- 113 M. G. Silveirinha, *Phys. Rev. B: Condens. Matter*, 2009, **79**, 153109.
- 114 J. Yao, Z. W. Liu, Y. M. Liu, Y. Wang, C. Sun, G. Bartal, A. Stacy and X. Zhang, *Science*, 2008, **321**, 930.
- 115 C. R. Martin, *Science*, 1994, **266**, 1961–1966.
- 116 H. Masuda and K. Fukuda, *Science*, 1995, **268**, 1466–1468.
- 117 A. Alu and N. Engheta, *Opt. Express*, 2004, **14**, 1557–1567.
- 118 Y. A. Urzhumov, G. Shvets, J. Fan, F. Capasso, D. Brandl and P. Nordlander, *Opt. Express*, 2007, **15**, 14129–14145.
- 119 J. A. Fan, C. Wu, K. Bao, J. Bao, R. Bardhan, N. J. Halas, V. N. Manoharan, P. Nordlander, G. Shvets and F. Capasso, *Science*, 2010, **328**, 1135–1138.
- 120 G. M. Whitesides and B. Grzybowski, *Science*, 2002, **295**, 2418–2421.
- 121 K. J. Stebe, E. Lewandowski and M. Ghosh, *Science*, 2009, **325**, 159–160.
- 122 J. Kastel, M. Fleischhauer, S. F. Yelin and R. L. Walsworth, *Phys. Rev. Lett.*, 2007, **99**, 073602.
- 123 Y. F. Chen, P. Fischer and F. W. Wise, *Phys. Rev. Lett.*, 2005, **95**, 067402.
- 124 A. A. Zharov, I. V. Shadrivov and Y. S. Kivshar, *Phys. Rev. Lett.*, 2003, **91**, 037401.
- 125 V. M. Agranovich, Y. R. Shen, R. H. Baughman and A. A. Zakhidov, *Phys. Rev. B: Condens. Matter*, 2004, **69**, 165112.
- 126 N. Lazarides, M. Eleftheriou and G. P. Tsironis, *Phys. Rev. Lett.*, 2006, **97**, 157406.
- 127 Y. M. Liu, G. Bartal, D. A. Genov and X. Zhang, *Phys. Rev. Lett.*, 2007, **99**, 153901.
- 128 N. M. Litchinister and V. M. Shalaev, *Laser Phys. Lett.*, 2008, **5**, 411–420.
- 129 M. W. Klein, C. Enkrich, M. Wegener and S. Linden, *Science*, 2006, **313**, 502–504.
- 130 I. V. Shadrivov, S. K. Morrison and Y. S. Kivshar, *Opt. Express*, 2006, **14**, 9344–9349.
- 131 B. N. Wang, J. F. Zhou, T. Koschny and C. M. Soukoulis, *Opt. Express*, 2008, **16**, 16058–16063.
- 132 T. Driscoll, H. T. Kim, B. G. Chae, B. J. Kim, Y. W. Lee, N. M. Jokerst, S. Palit, D. R. Smith, M. Di Ventra and D. N. Basov, *Science*, 2009, **325**, 1518–1521.
- 133 V. V. Cheianov, V. Fal'ko and B. L. Altshuler, *Science*, 2007, **315**, 1252–1255.
- 134 S. Zhang, D. A. Genov, C. Sun and X. Zhang, *Phys. Rev. Lett.*, 2008, **100**, 123002.
- 135 Z. Jacob, J. Y. Kim, G. V. Naik, A. Boltasseva, E. E. Narimanov and V. M. Shalaev, *Appl. Phys. B: Lasers Opt.*, 2010, **100**, 215–218.
- 136 M. A. Noginov, H. Li, Y. A. Barnakov, D. Dryden, G. Nataraj, G. Zhu, C. E. Bonner, M. Mayy, Z. Jacob and E. E. Narimanov, *Opt. Lett.*, 2010, **35**, 1863–1865.
- 137 C. Henkel and K. Joulain, *Europhys. Lett.*, 2005, **72**, 929–935.
- 138 U. Leonhardt and T. G. Philbin, *New J. Phys.*, 2007, **9**, 254.
- 139 F. S. S. Rosa, D. A. R. Dalvit and P. W. Milonni, *Phys. Rev. Lett.*, 2008, **100**, 183602.
- 140 R. Zhao, J. Zhou, T. Koschny, E. N. Economou and C. M. Soukoulis, *Phys. Rev. Lett.*, 2009, **103**, 103602.
- 141 V. Yannopoulos and N. V. Vitanov, *Phys. Rev. Lett.*, 2009, **103**, 120401.
- 142 S. I. Maslovski and M. G. Silveirinha, *Phys. Rev. A*, 2010, **82**, 022511.